ELSEVIER

Catalysis Today 40 (1998) 181–190

CATALYSIS TODAY

Comparative study of the catalytic partial oxidation of methane to synthesis gas in fixed-bed and fluidized-bed membrane reactors

Part I: A modeling approach

T. Ostrowski [a], A. Giroir-Fendler [b], C. Mirodatos [b], L. Mleczko [a,*]

[a] *Lehrstuhl für Technische Chemie, Ruhr-Universität Bochum, D-44780 Bochum, Germany*
[b] *Institut de Recherches sur la Catalyse, CNRS, F-69626 Villeurbanne-Cédex, France*

Abstract

Catalytic partial oxidation of methane (CPOM) to synthesis gas over a Ni/α-Al_2O_3 catalyst in fixed-bed and fluidized-bed reactors with and without membranes was investigated by means of mathematical modeling and simulations. The reactors were simulated by applying conditions which are of relevance for industrial applications (p=5 and 30 bar, T=750–800°C). Since, at high pressures, the performance of a fixed-bed reactor for the CPOM reaction was strongly influenced by the intraparticle mass-transport limitation, the yield of syngas in fluidized-bed reactor was higher compared to the fixed-bed reactor. In both reactor types, the conversion of methane and yield of syngas could be significantly improved by means of integrated product separation on applying porous membranes. Due to the higher selectivity of separation the membrane fluidized bed was superior to the fixed bed. In turn, the higher selectivity of separation in fluidized-bed membrane reactors was attributed to the mass-transfer limitation between the bubble and emulsion phases that acted as a prefiltering membrane. However, the improvement of the selectivity of separation due to the interphase gas exchange decreased with increasing pressure. © 1998 Elsevier Science B.V.

1. Introduction

Attempts have been made in recent years to improve carbon and thermal efficiency and to reduce investment costs of reformers for the synthesis gas production. In order to achieve these goals, the catalytic partial oxidation of methane to synthesis gas (CPOM, see Eq. (1)) has been proposed as an alternative to the commonly applied steam-reforming process [1].

$$CH_4 + 0.5O_2 \rightarrow CO + 2H_2$$
$$\Delta_r H_{1000\,K} = -21.8\,kJ/mol \quad (1)$$

In spite of the intensive research, the CPOM process is still in the precompetitive stage of development. The most important limitation for making this reaction commercially viable is given by the thermodynamics, i.e. the increase of pressure, required for down-stream processes like methanol or Fischer–Tropsch synthesis, leads to low equilibrium methane conversions. The dependence of the equilibrium methane conversion (see Fig. 1) on temperature and pressure was calculated by applying the process simulation software ASPEN-PLUS™. The equilibrium concentration

*Corresponding author. Present address: BAYER AG, ZT-TE Geb E41, D-51368 Leverkusen; fax: +214/305 0262; e-mail: LESLAW.MLECZKO.LM@bayer-ag.de

PII S0920-5861(98)00006-6

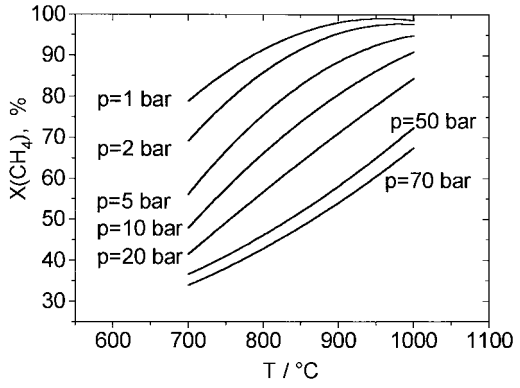

Fig. 1. Equilibrium methane conversions for temperatures between 700 and 1000°C for pressures between 1 and 70 bar (calculated with the ASPEN-PLUS™ software [2]).

was calculated in two steps. In the first step, stoichiometric combustion of methane was assumed; in the second step, the equilibrium composition was calculated taking into account steam and dry reforming as well as the water–gas shift reaction. In order to overcome the thermodynamic limitation membrane reactors were proposed (e.g. [3,4]). However, when performing this reaction in a catalytic fixed-bed membrane reactor, high temperature spikes and catalyst deactivation due to carbon deposition occurred [3]. In order to eliminate these drawbacks a fluidized-bed membrane reactor has been proposed [5]. In this reactor type, integrated product separation by means of porous ceramic or dense metal membranes leads to higher methane conversions and syngas yields. Furthermore, the intensive mixing of solid particles in the fluidized bed could be utilized for achieving isothermal conditions and continuous catalyst regeneration (see [6]). Previous simulations performed for the industrial-scale, atmospheric-pressure membrane fluidized-bed reactor showed that, in this reactor type, methane conversion and syngas yield above the thermodynamic equilibrium, can be achieved. Furthermore, even when applying porous membranes, high selectivities of hydrogen separation were predicted. These high selectivities of separation might be explained by the limitation for the gas exchange between the bubble and emulsion phases that resulted in the equilibrium composition of gas, i.e. high concentration of hydrogen and carbon monoxide, in the emulsion phase [7]. However, the selectivity of gas separation and, in turn, the yield of synthesis gas strongly depended on the thermodynamic and hydrodynamic conditions.

The work reported in this paper aimed at predictions of the catalytic performance of an industrial-scale fluidized-bed membrane reactor operated at elevated pressure. Furthermore, performances of the fixed-bed and fluidized-bed membrane reactors have been compared. In order to achieve these goals, reaction engineering models of both types of membrane reactors were developed and simulations were performed by applying conditions which are of relevance for industrial use. Special attention in these simulations was put to the analysis of the effect of bed hydrodynamics and multicomponent diffusion on the selectivity of separation.

2. Modeling

2.1. Kinetics

The rates of the chemical reactions were calculated by applying the kinetic model, proposed by de Groote and Froment [8], for the CPOM reaction. This kinetic model was developed for describing the reaction at high temperatures and pressures (T>700°C, p>25 bar) over a Ni/α-Al_2O_3 catalyst. The reaction network consisted of combustion of methane (2), steam reforming to CO (3) and CO_2 (4), and water–gas shift reaction (5):

$$CH_4 + 2O_2 \rightarrow CO_2 + 2H_2O \quad (2)$$

$$CH_4 + H_2O \rightleftharpoons CO + 3H_2 \quad (3)$$

$$CH_4 + 2H_2O \rightleftharpoons CO_2 + 4H_2 \quad (4)$$

$$CO + H_2O \rightleftharpoons CO_2 + H_2 \quad (5)$$

The rate equations as well as the kinetic parameters applied for the calculation of the reaction rates are summarized in Tables 1–3. For the sake of simplicity (and in agreement with the experimental results, see [7]), the influence of carbon deposition due to the Boudouard reaction and the cracking of methane on the catalyst activity were neglected.

2.2. Membranes

Porous ceramic membranes or porous stainless-steel membranes were proposed for the application in high-temperature CPOM reactors. Knudsen diffu-

Table 1
Reaction rate equations and the effectiveness factors for the catalyst particles applied in industrial fixed-bed reactors

Reaction	Rate equation	Effectiveness factor η [8]
$CH_4+2O_2 \rightarrow CO_2+2H_2O$	$r_1 = \frac{k_1 x_{CH_4} x_{O_2}}{(1 + K^c_{CH_4} x_{CH_4} + K^c_{O_2} x_{O_2})} + \frac{k_2 x_{CH_4} x_{O_2}^{1/2}}{(1 + K^c_{CH_4} x_{CH_4} + K^c_{O_2} x_{O_2})^2}$	0.05
$CH_4+H_2O \rightleftharpoons CO+3H_2$	$r_2 = \frac{k_3/p_{H_2}^{2.5}(p_{CH_4}p_{H_2O} - p_{H_2}^3 p_{CO}/K_{eq,3})}{(1 + K_{CO}p_{CO} + K_{H_2}p_{H_2} + K_{CH_4}p_{CH_4} + K_{H_2O}p_{H_2O}/p_{H_2})^2}$	0.07
$CO+H_2O \rightleftharpoons CO_2+H_2$	$r_3 = \frac{k_4/p_{H_2}(p_{CO}p_{H_2O} - p_{H_2}p_{CO_2}/K_{eq,4})}{(1 + K_{CO}p_{CO} + K_{H_2}p_{H_2} + K_{CH_4}p_{CH_4} + K_{H_2O}p_{H_2O}/p_{H_2})^2}$	0.70
$CH_4+2H_2O \rightleftharpoons CO_2+4H_2$	$r_4 = \frac{k_5/p_{H_2}^{3.5}(p_{CH_4}p_{H_2O}^2 - p_{H_2}^4 p_{CO_2}/K_{eq,5})}{(1 + K_{CO}p_{CO} + K_{H_2}p_{H_2} + K_{CH_4}p_{CH_4} + K_{H_2O}p_{H_2O}/p_{H_2})^2}$	0.06

Table 2
Kinetic parameters

Reaction	k_i (kmol(kg_{cat} s)$^{-1}$)	E_A (kJ mol^{-1})
1	$k_1=3.14\times10^{-7}$	—
	$k_2=2.64\times10^{-7}$	—
2	4.225×10^{15} bar$^{-0.5}$	240.1
3	1.995×10^{6} bar^{-1}	67.13
4	1.020×10^{15} bar$^{-0.5}$	243.9

Table 3
Adsorption constants

Component	K_o (bar^{-1})	ΔH_{ads} (kJ mol^{-1})
CH_4 (combustion)	6.67×10^{-7} bar	—
O_2 (combustion)	4.34×10^{-5} bar	—
CH_4	6.65×10^{-4}	−38.28
CO	8.23×10^{-5}	−70.65
H_2	6.12×10^{-9}	−82.90
H_2O	1.77×10^{5} bar	+88.68

sion was assumed for all gases permeating through the membrane. The validity of this assumption was checked by calculating the Knudsen number [9]. The contributions of pore flow, molecular sieving and surface diffusion were neglected. The gas-flow rates of the gases (Eq. (6)) were calculated by applying the values proposed by Wu and Liu [10] for the structural parameters of tortuosity and porosity. These parameters characterize the non-ideal pore structure of a real membrane. Since the permeation rate depended on the thickness of the separation layer, an asymmetric membrane geometry consisting of the separation layer on a macroporous support was assumed.

$$\dot{n}_{sep,P,j} = \frac{2 r_{po} \varepsilon_p}{3\tau RT \delta_{mem}} \cdot \sqrt{\frac{8RT}{\pi M_j}} \cdot (p_{P,j,r} - p_{P,j,s}) A_{mem,s} \tag{6}$$

2.3. Mass-balance equations for the fixed-bed membrane reactor

The simulations of the industrial fixed-bed membrane reactor (d=0.8 m) were carried out by applying a homogeneous one-dimensional model of the catalytic bed [11]. The model took into account that the gas velocity in the reactor was influenced by the reaction (change of molar flow rate) and by the separation of gas. The influence of intraparticle mass-transfer limitations was taken into account by applying effectiveness factors for the catalyst as proposed by de Groote and Froment ([8], see Table 1). Finally, isothermal conditions were assumed. The mass balance for the fixed-bed membrane reactor is given in Eq. (7).

$$\frac{d(c_j u)}{dz} = \sum_{k=1}^{NR} \eta_k \nu_{j,k} r_k (1-\varepsilon)\rho_{cat} - \frac{\dot{n}_{sep,P,j}}{A_T} \tag{7}$$

2.4. Mass-balance equations for the fluidized-bed membrane reactor

The model of the fluidized-bed membrane reactor presents a further development of the Bubble Assem-

blage Model [12]. According to the two-phase theory of fluidization [13], the bed was divided into the bubble and emulsion phases. The gas flowed through the emulsion phase with the minimum fluidization velocity (u_{mf}). The remaining gas ($u-u_{mf}$) flowed as bubbles. The bubbles were generated directly above the gas distributor and their diameters changed due to coalescence and splitting. Between both phases, mass transfer took place. All hydrodynamic parameters and the mass-transfer coefficient depended on the height above the distributor. This dependence was discretized in the model by dividing the reactor axially into a series of segments. The height of the segments corresponded to the local bubble diameter. In the fluidized-bed reactor, the separation by means of membranes took place from both phases, depending on the membrane area (ρ) being in contact with each phase. The division of the membrane area between both the phases depended on the local bubble hold-up (ε_B). Since the model took into account the change of the gas velocity due to the reaction and separation, an additional interphase gas-exchange term was introduced ($\dot{n}_{conv,BE,j,i}$) to correct the gas velocity in the emulsion phase which had to be kept on u_{mf}. The resulting mass balances for the emulsion and bubble phases are given in Eqs. (8) and (9).

Emulsion:

$$A_T u_{mf}[c_{E,j,i-1} - c_{E,j,i}] + k_{BE,i}V_{B,i}[c_{B,j,i} - c_{E,j,i}] - (1-\varepsilon_{B,i})\dot{n}_{sep,E,j}\Delta h_i + \sum_{k=1}^{NR} v_{j,k}r_{E,i,k} \times (1-\varepsilon_{mf})\rho_{cat}V_{E,i} - \dot{n}_{conv,BE,j,i} = 0 \quad (8)$$

Bubble:

$$A_T[(u_{i-1}-u_{mf})c_{B,j,i-1} - (u_i - u_{mf})c_{B,j,i}] - k_{BE,i}V_{B,i}[c_{B,j,i} - c_{E,j,i}] - \varepsilon_{B,i}\dot{n}_{sep,E,j}\Delta h_i + \sum_{k=1}^{NR} v_{j,k}r_{B,i,k}(1-\varepsilon_{mf})\rho_{cat}V_{C,i}) - \dot{n}_{conv,BE,j,i} = 0$$

$j = CH_4, O_2, CO_2, H_2O, CO, H_2;$

$i = 1 \ldots$ number of segments

Correlations used for calculations of hydrodynamic parameters and gas-exchange coefficients are presented elsewhere [5].

3. Simulation results and discussion

3.1. Effect of the integrated product separation on catalytic performance of a fixed-bed and a fluidized-bed reactor

In order to investigate the effect of the integrated product separation on the catalytic performance, comparative simulations for fixed-bed and fluidized-bed reactors operated at 750 and 800°C were carried out. Other reaction conditions applied in simulations, presented in this paper, are summarized in Table 4. The conversions and yields were calculated from cumulated outlet streams from the catalytic bed and from the membrane.

Since in both the reactors the reaction was strongly influenced by the mass-transport effects, at all investigated reaction conditions, syngas yields were lower than the equilibrium ones. Calculations performed at 750°C and 30 bar indicated that, in order to obtain the equilibrium conversion of methane which amounts to 44%, the contact time in the fixed-bed reactor had to be increased from 1.6 to 9.5 gs/ml (STP). This is a significant difference compared to the micro-catalytic reactors for which equilibria at significantly shorter contact times were reported (e.g. [14]). In the

Table 4
Conditions assumed for the simulations

		Fixed-bed	Fluidized-bed
Reactor:			
Diameter	m	0.8	4
Particle diameter	mm	16	0.1
Catalyst mass	kg	20000	20000
Gas distributor, openings	—	—	Perforated plate, 800 m^{-2}
Membranes:			
Pore diameter	nm	4	4
Thickness	μm	20	20
Tortuosity	—	3	3
Porosity	—	0.5	0.5
Permeation area	m^2	140	140
Conditions:			
Temperature	°C	750–800	750–800
Pressure	bar	5, 30	5, 30
$x_{CH_4} : x_{O_2} : x_{H_2}$	—	0.66 : 0.33 : 0.01	0.66 : 0.33 : 0.01
Inlet gas velocity	ms^{-1}	6.25	0.25

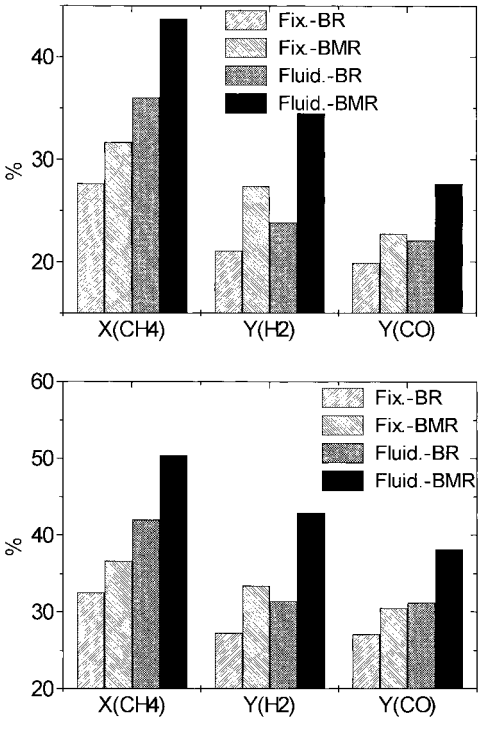

Fig. 2. Conversions of methane and yields of hydrogen and carbon monoxide predicted in various reactors at (a) 750°C and (b) 800°C (p=30 bar, Fix.-B(M)R: fixed-bed (membrane) reactor, Fluid.-B(M)R: fluidized-bed (membrane) reactor).

fluidized-bed reactor operated at gas velocity of $u_{800^\circ C}$=0.25 m/s, i.e. vigorously bubbling bed (u_0/u_{mf}=74), the height of the settled bed H_{mf} had to be increased from 1.6 to 6 m.

The conversion of methane and yields of CO and H_2, predicted for the fixed bed and fixed-bed membrane reactors as well as for the fluidized bed and fluidized-bed membrane reactors, are presented in Fig. 2. Higher conversions of methane and syngas yields were predicted for the fluidized-bed reactors compared to the fixed beds at both investigated temperatures 750 (Fig. 2a) and 800°C (Fig. 2b). These calculations indicate that the intraparticle mass-transport limitation in the fixed-bed reactors (η=0.04−0.06 for the reforming steps, η=0.70 for the water–gas shift reaction) affected the catalytic performance than the limitation for the gas exchange between the bubble and emulsion phases. Similar results were reported for the steam reforming of methane [15]. Since in the fluidized bed small particles were applied compared to those in the fixed bed, the effect of the pore diffusion limitation on the reaction rate could be neglected; the Thiele-modulus [16] estimated for the particles used in the fluidized bed amounted to 10^{-2}–10^{-4}.

When immersing porous membranes in the catalytic bed, conversion of methane as well as yield of CO and H_2 significantly increased in both the reactor types (see Fig. 2). The highest conversions and yields were calculated for the fluidized-bed membrane reactor. Furthermore, the increase of conversion and yields was more pronounced for the fluidized-bed membrane reactor than for the fixed-bed one. In order to explain this effect the selectivities of separation calculated for both reactors were analyzed. The selectivity of separation was defined as the concentration of the components in the sweep gas relatively to the hydrogen concentration (c_{H_2} was set to 1). The concentrations of methane, carbon dioxide and carbon monoxide in the sweep gas of the fixed bed were higher than the concentrations of these components in the permeate of the fluidized-bed membrane reactor (see Fig. 3). Especially, the high permeation rate of methane was detrimental for high syngas yields since methane bypasses the catalytic bed in the sweep gas and, therefore, cannot be converted by the reforming reactions.

3.2. Concentration profiles

In order to elucidate the effect of the integrated product separation, the reaction pathway concentration profiles in the catalytic beds were analyzed. Simulations were performed for the reactors operating at 750°C and 30 bar.

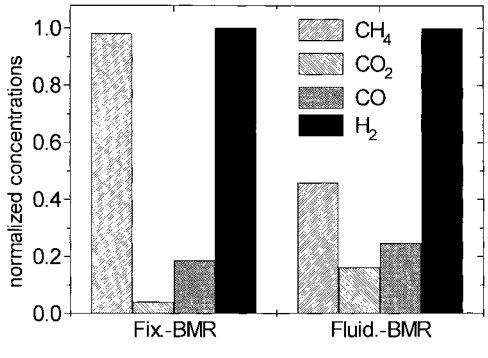

Fig. 3. Concentrations of methane, carbon dioxide and carbon monoxide relative to the hydrogen concentration in various reactor types at 750°C.

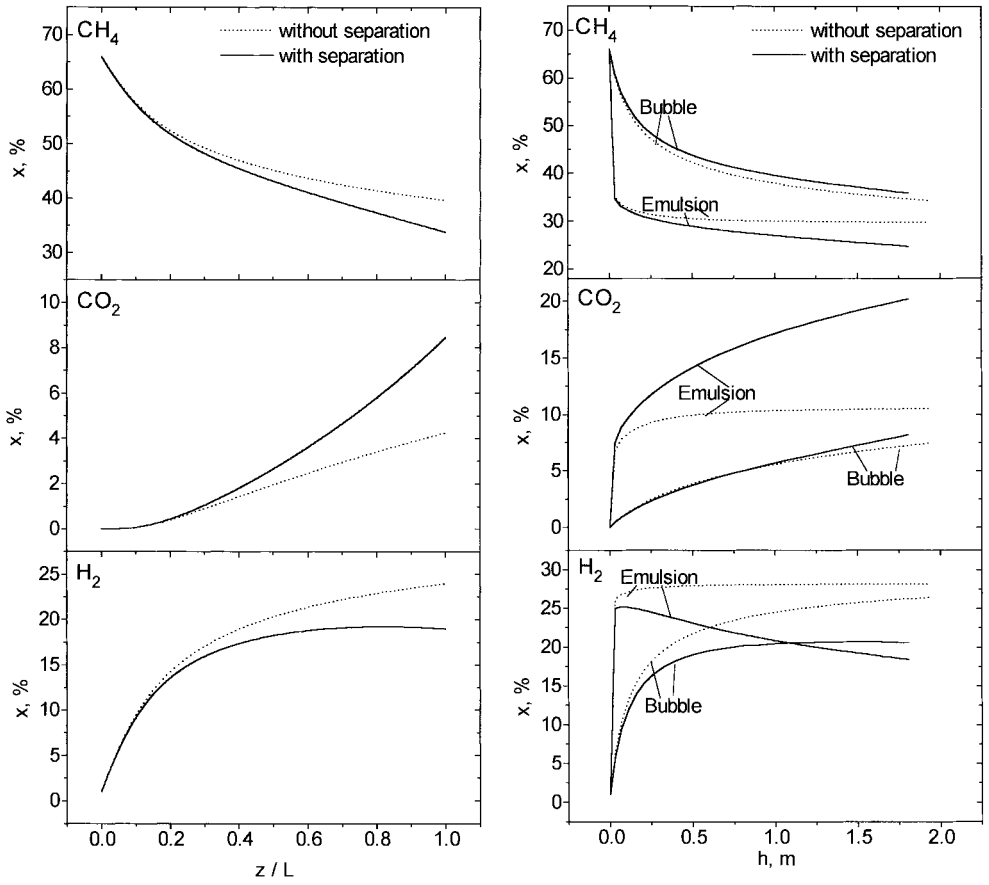

Fig. 4. Concentration profiles of methane, carbon dioxide and hydrogen predicted for the (a) fixed-bed and (b) fluidized-bed reactors at 750°C (p=30 bar, dotted-lines: without product separation, straight lines: with product separation).

In the fixed-bed reactor the molar fractions of methane and oxygen (not shown) decreased exponentially along the reactor axis (see Fig. 4a, dotted lines). Since the rate of the combustion reaction was strongly influenced by the intraparticle mass-transport limitations, complete conversion of oxygen was not achieved. The final products, carbon monoxide (not shown) and hydrogen increased strongly with the contact time. Since the mass-transport limitation affected the combustion of methane (η=0.05) more strongly than the reforming reactions (η=0.06-0.07), the profiles of the desired products CO and H_2 were symmetrical to the ones of methane and oxygen. Furthermore, the molar fractions of the intermediate products carbon dioxide and water were kept in the whole reactor on low level compared to the ones of hydrogen and carbon monoxide by the reforming steps.

When porous membranes were placed on the whole length of the catalytic bed the high concentrations of feedstocks and the low ones of products in the front-end of the fixed-bed reactor promoted permeation of methane and intermediate products (see Fig. 4a, straight lines). The non-selective separation mainly of methane and water, in turn, caused an additional drop of the concentrations of these products in the catalytic bed. The integrated separation of gas promoted the conversion of methane and syngas yield first in this part of the reactor which was characterized by a high concentration of products, i.e. in the back-end part of the reactor. Therefore, it can be postulated that in order to achieve high selectivities of separation in

fixed-bed reactors and, in turn, significant improvement of conversion of methane and yield to synthesis gas porous membranes should not be placed on the whole reactor length. The separation should take place only in that part of the reactor where the gas composition approached the thermodynamic equilibrium. The strong increase of carbon dioxide molar fraction predicted in the fixed-bed membrane reactor could be explained by the enrichment effect.

In the fluidized-bed reactor the composition of gas in the emulsion phase was almost constant (see Fig. 4b). This was attributed to the mass-transport limitation between the bubble and emulsion phases. Furthermore, the molar fractions of reactants in the emulsion phase were low and the ones of products were high. However, the concentrations of reactants in the emulsion phase were significantly higher compared to the ones predicted for the atmospheric-pressure fluidized-bed reactor [7]. This could easily be explained by the fact that the reaction in the emulsion phase approached the thermodynamic equilibrium and the equilibrium conversion of methane decreased with the pressure (see Fig. 1). In bubbles, the profiles were similar to those in the fixed bed, i.e. the molar fractions of methane and oxygen were high at the reactor entrance and decreased with the distance from the gas distributor (see Fig. 4b). In turn, the concentrations of desired products H_2 and CO increased with the height in the bed. However, at all positions, the product molar fractions in the emulsion were lower than the ones in the bubbles.

The integrated product separation predominantly influenced the gas composition in the emulsion phase since ca. 80% of the membrane area was in contact with this phase. In the emulsion phase the molar fraction of hydrogen significantly decreased with the height, especially in the upper part of the bed. Also the molar fraction of hydrogen in bubbles was lower than in the fluidized-bed reactor without membranes. The mass-transport limitation between both phases promoted a high selectivity of separation since the membranes immersed in the fluidized bed interacted mainly with the gas in the emulsion phase; it acted as a prefiltering membrane. However, the improvement of the selectivity of separation was lower than in the atmospheric pressure reactor because the molar fraction of methane and intermediate products in this phase was significantly higher than at the atmospheric pressure. Therefore, it can be deduced that the increase of the syngas yield in the fluidized-bed reactor equipped with porous membranes would decline with increasing pressure in the reactor. Against this background, the application of (asymmetric) Pd-membranes for performing the CPOM reaction at high pressures that was found in our pervious study to be less promising [5] and was already successfully applied for steam reforming reaction [17] has to be reconsidered.

3.3. Sensitivity analysis

Two effects influenced the accuracy of the simulation results reported in this paper: (i) the kinetics of the methane combustion was developed [18] for a different catalyst (Pt/Al_2O_3) and for different reaction conditions, and (ii) the deviation of the gas withdraw by means of porous membranes due to non-Knudsen flow was neglected. The influence of these two effects on reactor performance will be analyzed in Sections 3.3.1 and 3.3.2.

3.3.1. Effect of kinetics

In order to investigate the effect of the rate of the combustion reaction on the conversion of methane, the rate constant for this reaction was increased by factor of 1 to 15. Results of this sensitivity analysis are presented in Fig. 5. The conversion of methane in the fluidized-bed reactor was almost independent of the combustion reaction rate since the mass transfer

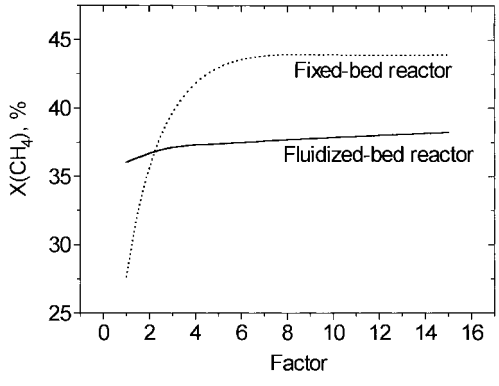

Fig. 5. Effect of the reaction velocity of the combustion step (characterized by the factor of the increase of the combustion step, factor=1: literature data) on methane conversion for the fixed-bed (· · ·) and the fluidized-bed reactor (———) at 750°C and 30 bar.

between the bubble and emulsion phases was the limitation step for the methane conversion (see concentration profiles). In contrast, as long as equilibrium was not achieved the methane conversion in the fixed-bed reactor strongly depended on the rate of the combustion step. When the reaction velocity was increased by the factor 5 thermodynamic equilibrium ($X_{CH_4} = 44\%$) was reached at the applied contact time (1.6 gs/ml). When increasing the activity of the catalyst for the combustion step, the conversion of methane in the fixed and fluidized-bed membrane reactor were higher than in the conventional reactors (4.5% for the fixed-bed membrane and 7.1% for the fluidized-bed membrane reactor). This indicates that, even when the rate for methane combustion was increased, the intraparticle mass-transfer limitations of the reforming steps in the fixed bed lead to worse separation selectivities and to a lower increase of syngas yield compared to the fluidized bed.

3.3.2. *Effect of non-Knudsen flow*

In order to describe gas separation through a porous membrane Knudsen diffusion was assumed. The validity of this approach for describing permeability of single component gases was confirmed experimentally [19]. However, for the case of multicomponent gas diffusion, selectivities of separation lower than that expected for the Knudsen diffusion were reported [9,19]. These differences were explained by the influence of support, surface diffusion and viscous flow. Additionally, the permeation through a membrane could be influenced by pinholes generated during the use or preparation of the membranes. In order to elucidate the sensitivity of the model predictions to the uncertainty in the calculation of the permeation rate, a parametric study was performed by decreasing the hydrogen permeation rate by factor of 0.5 compared to the one calculated for the Knudsen diffusion.

The predicted conversions of methane in fixed-bed and fluidized-bed reactors, operated at a temperature of 750°C and pressures of 5 and 30 bar, are presented in Fig. 6. At 5 bar (Fig. 6a), the conversion of methane calculated for the fixed bed was higher than in the fluidized-bed reactor. However, at 30 bar (Fig. 6b) a higher conversion of methane was predicted for the fluidized-bed reactor. This result confirmed previous conclusions that at high pressures the conversion was more influenced by intraparticle mass-transport limitation in the fixed bed than interphase gas exchange in the fluidized-bed reactor. When the selectivity of gas withdraw corresponded to the Knudsen law ($S_{sep}=S_K$), the integrated gas separation caused a significant increase of methane conversion in both reactor types. However, in the case of lower separation selectivity ($S_{sep}=0.5S_K$), the conversion of methane in the fixed-bed membrane reactor dropped below the one obtained in the conventional fixed-bed reactor. Also, in the fluidized-bed membrane reactor conversion of methane dropped with decreasing selectivity of separation. However, even in the worst investigated case the conversion of methane in the fluidized-bed membrane reactor was higher than in the conventional fluidized bed. The prefiltering effects of the gas exchange between the bubble and emulsion phases could explain why the fluidized-bed membrane reactor was less sensitive to the separation selectivity than the fixed-bed one.

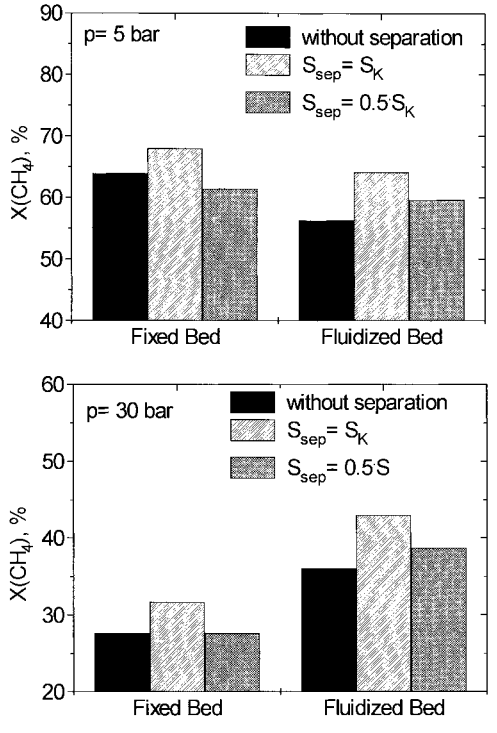

Fig. 6. Methane conversions predicted for fixed-bed and fluidized-bed reactors assuming Knudsen separation selectivity ($S_{sep}=S_K$) and reduced separation selectivity ($S_{sep}=0.5S_K$) for (a) 5 and (b) 30 bar (T=750°C).

The calculated concentrations of methane, carbon dioxide and carbon monoxide relative to hydrogen in the permeate confirmed the above proposed explanation with respect to the effect of the interphase mass-transport limitation and reaction pressure on the syngas yield in the membrane reactor equipped with porous membranes. The concentration of methane in the permeate of the fixed-bed membrane reactor was always significantly higher than in the fluidized-bed membrane reactor. Furthermore, the concentration of methane in the permeate was less sensitive to the reaction pressure in the fluidized bed than in the fixed-bed membrane reactor. Methane was the main non-selectively separated component in the permeate gas. This was due to its low molecular weight compared to other reactants and products. Furthermore, it was available in a high concentration, at least in the entrance zone of the reactor. Carbon monoxide is also separated at a rate comparable to that for methane. In all investigated cases, the concentration of carbon dioxide and water was lower than those of methane and carbon monoxide. From the safety point of view it was important that the concentration of oxygen in the permeate was negligible.

4. Conclusions

Mathematical models of catalytic partial oxidation of methane to synthesis gas in the fixed-bed and fluidized-bed as well as fixed-bed and fluidized-bed membrane reactors, equipped with porous membranes, were applied for predicting the performance of these reactors when performing the CPOM reaction at elevated pressures. Although the predictions suffer from the limited accuracy of the applied kinetics, the performed simulations illustrate the effect of different hydrodynamic conditions in a fixed bed and in a fluidized bed, as well as the influence of the pressure on the performance of membrane reactors.

Since at high pressures (30 bar) the performance of a fixed-bed reactor for the CPOM reaction was strongly influenced by the intraparticle mass-transport limitation, the yield of syngas in the fluidized-bed reactor was higher compared to one in the fixed-bed reactor. Furthermore, the results of simulations performed for both reactor types confirmed that the conversion of methane and the yield of syngas could be significantly improved by means of integrated product separation. The higher selectivity of separation in fluidized-bed membrane reactors was attributed to the mass-transfer limitation between the bubble and emulsion phases that acted as a prefiltering membrane. The promoting effect of the interphase gas exchange decreased, however, when the pressure in the reactor increased. The performed sensitivity analysis showed that the performance of the fixed-bed reactor strongly depended on the reaction velocity of the initial methane combustion; in the fluidized-bed reactor the mass-transfer limitation between both phases was mainly responsible for the conversion. Additionally, the decrease of separation selectivity had a detrimental effect for the reactor performance; integrated gas separation could even result in the decreased conversion of methane. The performance of a fluidized-bed membrane reactor was less sensitive to the selectivity of separation compared to the fixed bed.

5. Notation

$A_{\mathrm{mem},s}$	specific membrane area, m^2/m
A_T	cross sectional reactor area, m^2
B	bubble phase (index), –
$c_{\mathrm{B},j,i}$	concentration of component j in the bubble phase at segment i, mol/m^3
$c_{\mathrm{E},j,i}$	concentration of component j in the emulsion phase at segment i, mol/m^3
d_{p}	particle diameter, m
E	emulsion phase (index), –
$\Delta_{\mathrm{r}}H_{1000\ \mathrm{K}}$	reaction enthalpy of reaction at 1000 K, J/mol
Δh_i	height of segment i, m
$K_{\mathrm{eq},1}$	thermodynamic equilibrium constant of reaction 1, dimension depends on reaction
K_j	adsorption constant for component j in reforming reactions, 1/bar
K_j^{c}	adsorption constant for component j in the combustion reaction, –
k_1	rate constant of reaction 1, depends on reaction
$k_{\mathrm{BE},i}$	mass-exchange coefficient between the bubble and emulsion phases at segment i, 1/s

M_j	molecular weight of component j, kg/mol
NR	number of reactions, -
$\dot{n}_{\mathrm{conv,BE},j,i}$	convective flow of component j at segment i between the bubble and emulsion phases, mol/s
$\dot{n}_{\mathrm{sep,P},j}$	specific rate of gas separation of component j in phase P, mol/(m·s)
p	total pressure, Pa
$p_{\mathrm{P},j,i,\mathrm{r}}$	partial pressure of component j at segment i in phase P on reaction side, Pa
$p_{\mathrm{P},j,i,\mathrm{s}}$	partial pressure of component j at segment i in phase P on sweep side, Pa
R	gas constant, J/(mol K)
$r_{\mathrm{P},i,k}$	rate of reaction k at segment i in phase P, mol/(kg s)
r_{po}	radius of membrane pore, m
S_{sep}	separation selectivity (S_{K}=Knudsen selectivity), –
T	temperature, °C, K
u_{mf}	minimum fluidisation velocity, m/s
u	gas velocity, m/s
u_i	gas velocity at segment i, m/s
u_{s}	sweep gas velocity, m/s
$V_{\mathrm{B},i}$	volume of bubble at segment i, m^3
$V_{\mathrm{C},i}$	volume of cloud phase at segment i, m^3
$V_{\mathrm{E},i}$	volume of emulsion phase at segment i, m^3
$X(CH_4)$	methane conversion, %
x_j	molar fraction of component j, %
$Y(H_2)$	yield of hydrogen, %
$Y(CO)$	yield of carbon monoxide, %
z/L	dimensionless reactor axis, –
δ_{mem}	membrane thickness, m
ε	porosity in the fixed-bed, –
ε_{p}	porosity of membrane, –
$\varepsilon_{\mathrm{mf}}$	porosity at minimum fluidization condition, –
$\varepsilon_{\mathrm{B},i}$	fraction of bed volume in bubbles in segment i, –
η_k	effectiveness factor of reaction k, –
ρ_{cat}	density of catalyst, kg/m^3
ξ	part of membrane area which is contacted to bubble phase, –
ν_{j1}	stoichiometric coefficient of component j, –
τ	tortuosity of membrane, –

Acknowledgements

L. Mleczko and T. Ostrowski would like to acknowledge the financial support from the Deutsche Forschungsgemeinschaft (Project No. Ml 5/2-1).

References

[1] J.D. Korchnak, M. Dunster, Reduced Methanol Production Costs, World Methanol Production Conference, San Francisco, 1987.
[2] Process Simulation Software ASPEN-PLUS™, Aspen Technology Inc., Release 8, Cambridge, 1988.
[3] A. Santos, J. Coronas, M. Menéndez, J. Santamaria, Catal. Lett. 30 (1995) 189.
[4] T. Ioannides, X.E. Verykios, Catal. Lett. 36 (1996) 165.
[5] L. Mleczko, T. Ostrowski, T. Wurzel, Chem. Eng. Sci. 51 (1996) 3187.
[6] L. Mleczko, T. Wurzel, Chem. Eng. J. 66 (1997) 193.
[7] T. Ostrowski, Ph.D. Thesis, Ruhr-University Bochum – in preparation.
[8] A.M. de Groote, G.F. Froment, Appl. Catal. A 138 (1996) 245.
[9] R. Datta, S. Dechapanichkul, J.S. Kim, L.Y. Fang, H. Uehara, J. Membr. Sci. 75 (1992) 245.
[10] J.C.S. Wu, P.K.T. Liu, Ind. Eng. Chem. Res. 31 (1992) 322.
[11] G.F. Froment, K.B. Bischoff, Chemical Reactor Analysis and Design, John Wiley and Sons, New York, Chichester, 1979.
[12] K. Kato, C.Y. Wen, Chem. Eng. Sci. 24 (1969) 1351.
[13] J.F. Davidson, D. Harrison, Fluidised Particles, Cambridge University Press, Cambridge, 1963.
[14] M. Huff, P.M. Torniainen, L.D. Schmidt, Catal. Today 21 (1994) 113.
[15] S.S.E.H. Elnashaie, A.M. Adris, Fluidization VI, in: J. Grace, W. Shelmit, M Beuvgnou (Eds.), AIChE, New York, 1989, p. 319.
[16] M. Baerns, H. Hofmann, A. Renken, Chemische Reaktionstechnik, Georg Thieme Verlag, Stuttgart, New York, 1987.
[17] A.M. Adris, S.S.E.H. Elnashaie, R. Hughes, Can. J. Chem. Eng. 69 (1991) 1061.
[18] D.L. Trimm, C. Lam, Chem. Eng. Sci. 35 (1980) 1413.
[19] M. Chai, M. Machida, K. Eguchi, H. Arai, J. Membr. Sci. 96 (1994) 205.